Langmuir
Article
pubs.acs.org/Langmuir

Self-Assembly of Symmetric Diblock Copolymers in Planar Slits with and without Nanopatterns: Insight from Dissipative Particle Dynamics Simulations

Pavel Petrus,[†,‡] Martin Lísal,*[,†,‡] and John K. Brennan[§]

[†]*Department of Physics, Faculty of Science, J. E. Purkinje University, Ústí n. Lab., Czech Republic,* [‡]*E. Hála Laboratory of Thermodynamics, Institute of Chemical Process Fundamentals of the ASCR, v. v. i., Prague 6-Suchdol, Czech Republic, and* [§]*U.S. Army Research Laboratory, Weapons and Materials Research Directorate, Aberdeen Proving Ground, Maryland 21005-5066*

Received August 27, 2009. Revised Manuscript Received October 3, 2009

We present a dissipative particle dynamics simulation study on the formation of nanostructures of symmetric diblock copolymers confined between planar surfaces with and without nanopatterns. The nanopatterned surface is mimicked by alternating portions of the surface that interact differently with the diblock copolymers. The formation of the diblock−copolymer nanostructures confined between the planar surfaces is investigated and characterized by varying the separation width and the strength of the interaction between the surfaces and the diblock copolymers. For surfaces with nanopatterns, we also vary both the mutual area and location of the nanopatterns, where we consider nanopatterns on the opposing surfaces that are vertically (a) aligned, (b) staggered, and (c) partially staggered. In the case of planar slits without nanopatterns, we observe the formation of perpendicular and parallel lamellar phases with different numbers of lamellae. In addition, the symmetric diblock copolymers self-assemble into adsorbed layer and adsorbed layer−parallel lamellar phases and a mixed lamellar phase when the opposing surfaces of the planar slits are modeled by different types of wall beads. In the case of nanopatterned planar slits, we observe novel nanostructures and attempt to rationalize the diblock copolymer self-assembly on the basis of the behavior that we observed in the planar slits without nanopatterns. In particular, we investigate the applicability of predicting the structures formed in the nanopatterned slits by a superposition of the observed structures in slits without nanopatterns.

1. Introduction

Diblock copolymers consist of two chemically incompatible blocks A and B that are connected end-to-end. When diblock copolymers are quenched under the order−disorder temperature, the A and B blocks tend to form separated phases; however, they are prevented from doing so by the end-to-end connectivity. Instead, the diblock copolymers self-assemble into nanostructures that minimize contacts between the A and B blocks. The morphology of the nanostructures depends on the length ratio of the two blocks and the strength of chemical incompatibility between the blocks. The natural tendency of diblock copolymers to self-organize on the mesoscale into dense, regular arrays of nanostructures makes them attractive for various nanotechnology-related applications.[1] In the bulk phase, diblock copolymer systems form four classical microphases: the lamellar phase for symmetric (where the lengths of the A- and B-blocks are equal) or slightly unsymmetric diblock copolymers and the cylindrical, gyroid, and micellar phases otherwise.[2] However, in confinement, adsorption interactions, symmetry breaking, structural frustration, confinement-induced entropy loss, and heterogeneous surfaces play a dominant role leading to nanostructures that differ from those found in the bulk. From a technological viewpoint, the intriguing prospects of diblock copolymer self-assembly in nanopatterned confinement are indeed the novel nanostructures that can form, but the possibility that they may serve as templates for other types of nanostructures is also intriguing.

Our understanding of the self-assembly of symmetric diblock copolymers confined between planar slits without nanopatterns continues to deepen via experimental, theoretical, and simulation studies;[3,4] for example, the influence of copolymer polydispersity was recently studied.[5] For these systems, typically each slit wall has a substantial preferential affinity toward one of the blocks, which results in lamellae aligning in a parallel orientation with respect to the walls as shown in Figure 1a. Ideally, the parallel lamellar phase adopts lamellae of thickness νW^0_{LAM}, where ν is an integer corresponding to the number of lamellae and W^0_{LAM} is the bulk-phase lamellar spacing. In cases where the natural spacing of the lamellae is incommensurate with the separation of the walls or slit width W (i.e., $W \neq \nu W^0_{\mathrm{LAM}}$ for any value of ν), a parallel phase would be too energetically and structurally frustrated. Thus, to avoid this situation the lamellae prefer to align perpendicular to the walls, as shown in Figure 1b. Whereas a perpendicular lamellar phase cannot accommodate the energetically favorable layering of the preferentially adsorbed block, its lamellae spacing is free to relax to its bulk-phase spacing. Lamellae can also orientate to a mixed lamellar phase, as shown in Figure 1c, with ν parallel lamellae adsorbed at one surface and perpendicularly orientated lamellae at the other surface. Although the presence of an interface between the two lamellae orientations is energetically costly, this cost is compensated for by the adsorbed layer at the wall. A mixed lamellar phase is slightly unstable with respect to a perpendicular lamellar phase; however, this morphology can be

*Corresponding author. E-mail: lisal@icpf.cas.cz.

(1) Xia, Y.; Rogers, J. A.; Paul, K. E.; Whitesides, G. M. *Chem. Rev.* **1999**, *99*, 1823–1848.
(2) Bates, F. S.; Frederickson, G. H. *Annu. Rev. Phys. Chem.* **1990**, *41*, 525–557.
(3) Binder, K. *Adv. Polym. Sci.* **1999**, *138*, 1–89.
(4) Fasolka, M. J.; Mayes, A. M. *Annu. Rev. Mater. Res.* **2001**, *31*, 323–355.
(5) Han, Y.; Cui, J.; Jiang, W. *Macromolecules* **2001**, *41*, 6239–6245.

Report Documentation Page

Form Approved
OMB No. 0704-0188

1. REPORT DATE	2. REPORT TYPE	3. DATES COVERED
03 OCT 2009		**00-00-2009 to 00-00-2009**

4. TITLE AND SUBTITLE	5a. CONTRACT NUMBER
Self-Assembly of Symmetric Diblock Copolymers in Planar Slits with and	5b. GRANT NUMBER
	5c. PROGRAM ELEMENT NUMBER
6. AUTHOR(S)	5d. PROJECT NUMBER
	5e. TASK NUMBER
	5f. WORK UNIT NUMBER
7. PERFORMING ORGANIZATION NAME(S) AND ADDRESS(ES) **E. Hala Laboratory of Thermodynamics,Institute of Chemical Process Findamentals of ASCR,v. v. i. Rozvojova 135,165 02 Prague 6-Suchdol, Czech Republic,**	8. PERFORMING ORGANIZATION REPORT NUMBER
9. SPONSORING/MONITORING AGENCY NAME(S) AND ADDRESS(ES)	10. SPONSOR/MONITOR'S ACRONYM(S)
	11. SPONSOR/MONITOR'S REPORT NUMBER(S)

12. DISTRIBUTION/AVAILABILITY STATEMENT
Approved for public release; distribution unlimited

13. SUPPLEMENTARY NOTES

14. ABSTRACT

15. SUBJECT TERMS

16. SECURITY CLASSIFICATION OF:			17. LIMITATION OF ABSTRACT	18. NUMBER OF PAGES	19a. NAME OF RESPONSIBLE PERSON
a. REPORT **unclassified**	b. ABSTRACT **unclassified**	c. THIS PAGE **unclassified**	**Public Release**	**15**	

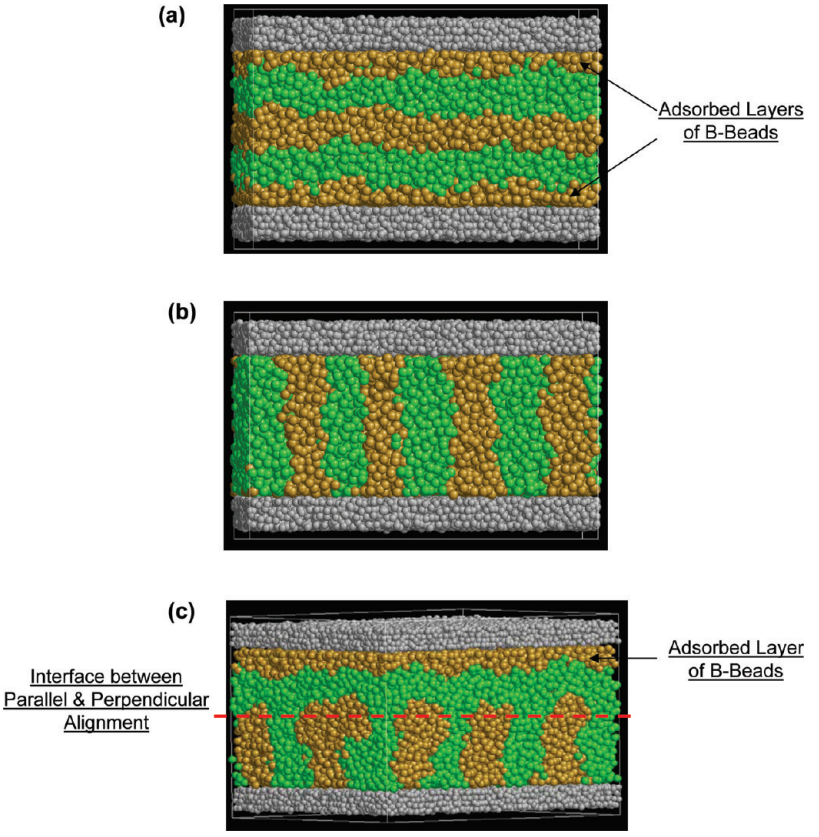

Figure 1. Examples of simulation configurations for (a) parallel, (b) perpendicular, and (c) mixed lamellar phases obtained by dissipative particle dynamics simulations of symmetric diblock copolymers A_5B_5 in planar slits without nanopatterns. Green and gold spheres represent A and B beads, respectively, whereas gray spheres represent wall beads. B beads have preferentially affinity for the walls and thus are adsorbed onto the walls.

preserved by imposing a small asymmetry between the copolymer block lengths.[6,7]

Similarly, many experimental, theoretical, and simulation studies have been performed on the self-assembly and adsorption of copolymers on nanopatterned surfaces; however, we are not aware of a systematic study involving symmetric diblock copolymers. A few notable computational studies are the work of Chen et al.,[8,9] where Monte Carlo simulations of the self-assembly of multiblock copolymers on nanopatterned surfaces were carried out. Also worth noting are the works of Genzer[10] and Semler and Genzer,[11] where a three-dimensional self-consistent-field model was used to study the adsorption of copolymers on planar substrates composed of two chemically distinct regions. These studies, as well as the recent experimental nanoassembly of symmetric diblock copolymers on chemically striped patterned surfaces,[12] demonstrate the strong influence of nanopatterns on the copolymer conformational and adsorption behavior as well as the ability of the copolymers to recognize the surface motif, which also contributes to the self-assembly.

In this work, we use the dissipative particle dynamics (DPD) method to explore the spontaneous nanostructure formation of symmetric diblock copolymers confined between planar surfaces both with and without nanopatterns. The surfaces are modeled as dense layers of DPD beads, where the nanopatterns are modeled by specifying alternating portions of the surface to interact differently with the diblock copolymers. The competition between the parallel and perpendicular lamellar alignments that occurs as a consequence of the nanopatterns leads to novel nanostructures. The self-assembly of nanostructures in planar slits is investigated and characterized by varying the slit width and the interaction between the walls and the diblock copolymers. For nanopatterned surfaces, we also varied both the mutual area and location of the nanopatterns, where we considered nanopatterns on the opposing surfaces that are vertically (a) aligned, (b) staggered, and (c) partially staggered. Qualitative phase diagrams are presented for the various systems along with the corresponding conformational behavior of the diblock copolymers. We make no attempt to locate the precise microphase separation boundaries; rather we attempt to quantify the various effects on self-assembly.

The remaining sections of the article are organized as follows. The simulation methodology is described in section 2, along with the DPD model of the confined diblock copolymer system and computational details. Results are discussed in section 3. Finally, section 4 gives our conclusions. Note that throughout the article we use the terms *surface* and *wall* interchangeably when describing the behavior in the planar slits.

2. Simulation Methodology

2.1. DPD for Confined Diblock Copolymer Systems. In our DPD simulations,[13,14] the diblock copolymer chain is

(6) Walton, D. G.; Kellogg, G. J.; Mayes, A. M.; Lambooy, P.; Russell, T. P. *Macromolecules* **1994**, *27*, 6225–6228.
(7) Matsen, M. W. *J. Chem. Phys.* **1997**, *106*, 7781–7791.
(8) Chen, H.; Peng, C.; Ye, Z.; Liu, H.; Hu, Y. *Langmuir* **2007**, *23*, 2430–2436.
(9) Chen, H.; Peng, C.; Sun, L.; Liu, H.; Hu, Y. *Langmuir* **2007**, *23*, 11112–11119.
(10) Genzer, J. *Macromol. Theory Simul.* **2002**, *11*, 481–493.
(11) Semler, J. J.; Genzer, J. *J. Chem. Phys.* **2003**, *119*, 5274–5280.
(12) Shin, D. O.; Kim, B. H.; Kang, J.-H.; Jeong, S.-J.; Park, S. H.; Lee, Y.-H.; Kim, S. O. *Macromolecules* **2009**, *42*, 1189–1193.
(13) Hoogerbrugge, P. J.; Koelman, J. M. V. A. *Europhys. Lett.* **1992**, *19*, 155–160.
(14) Koelman, J. M. V. A.; Hoogerbrugge, P. J. *Europhys. Lett.* **1993**, *21*, 363–368.

modeled as a collection of point beads that represent lumps of the chain containing several segments.[15] Confining walls are modeled by creating dense layers of DPD beads that represent several atoms, where the DPD beads can be arranged either randomly[16] or on a lattice.[17] The density of the wall layers must be sufficiently large to avoid penetration of the diblock copolymer beads into these confining walls.

In this study, all DPD beads are defined by a mass m_i, position $\mathbf{r}_i$, and velocity $\mathbf{v}_i$, and interact with each other via a pairwise, two-body, short-ranged force $\mathbf{F}$ that is written as the sum of a conservative force $\mathbf{F}^{\mathrm{C}}$, dissipative force $\mathbf{F}^{\mathrm{D}}$, and random force $\mathbf{F}^{\mathrm{R}}$:

$$\mathbf{F}_{ij} = \mathbf{F}_{ij}^{\mathrm{C}} + \mathbf{F}_{ij}^{\mathrm{D}} + \mathbf{F}_{ij}^{\mathrm{R}} \tag{1}$$

For the linear diblock copolymer chains, $\mathbf{F}^{\mathrm{C}}$ includes a soft repulsion force, $\mathbf{F}^{\mathrm{Cr}}$, acting between two nonbonded beads and a harmonic spring force, $\mathbf{F}^{\mathrm{Cs}}$, acting between bonded beads in a chain. The DPD diblock copolymer chains are flexible because no additional constraints such as bond bending or bond torsion are included. For a wall bead, $\mathbf{F}^{\mathrm{C}}$ contains, in addition to $\mathbf{F}^{\mathrm{Cr}}$, a wall force $\mathbf{F}^{\mathrm{Cw}}$ that tethers a wall bead to its initial position $\mathbf{r}_{\mathrm{w}}$. Expressions for $\mathbf{F}^{\mathrm{Cr}}$, $\mathbf{F}^{\mathrm{Cs}}$, and $\mathbf{F}^{\mathrm{Cw}}$ are given by

$$\mathbf{F}_{ij}^{\mathrm{C}} = \begin{cases} a_{ij}\left(1-\frac{r_{ij}}{r_{\mathrm{c}}}\right)\frac{\mathbf{r}_{ij}}{r_{ij}} & r_{ij} < r_{\mathrm{c}} \\ 0 & r_{ij} \geq r_{\mathrm{c}} \end{cases} \tag{2}$$

$$\mathbf{F}_{ij}^{\mathrm{Cs}} = -K_{\mathrm{s}}(r_{ij} - r_0)\frac{\mathbf{r}_{ij}}{r_{ij}} \tag{3}$$

and.

$$\mathbf{F}_{i}^{\mathrm{Cw}} = -K_{\mathrm{w}}(\mathbf{r}_i - \mathbf{r}_{\mathrm{w},i}) \tag{4}$$

respectively. In eqs 2−4, a_{ij} is the maximum repulsion between bead i and bead j, $\mathbf{r}_{ij} = \mathbf{r}_i - \mathbf{r}_j$, $\mathbf{r}_{ij} = |\mathbf{r}_{ij}|$, r_{c} is the cutoff radius, K_{s} is the spring constant, r_0 is the equilibrium spring length, and K_{w} is the wall-bead tethering constant.

The remaining two forces $\boldsymbol{F}^{\mathrm{D}}$ and $\boldsymbol{F}^{\mathrm{R}}$ are given by

$$\mathbf{F}_{ij}^{\mathrm{D}} = -\gamma_{ij}\omega^{\mathrm{D}}(r_{ij})\left(\frac{\mathbf{r}_{ij}}{r_{ij}}\cdot\mathbf{v}_{ij}\right)\frac{\mathbf{r}_{ij}}{r_{ij}} \tag{5}$$

$$\mathbf{F}_{ij}^{\mathrm{R}} = \sigma_{ij}\omega^{\mathrm{R}}(r_{ij})\frac{\zeta_{ij}}{\sqrt{\Delta t}}\frac{\mathbf{r}_{ij}}{r_{ij}} \tag{6}$$

where $\omega^{\mathrm{D}}(r_{ij})$ and $\omega^{\mathrm{R}}(r_{ij})$ are the weight functions that vanish for $r_{ij} \geq r_{\mathrm{c}}$, γ_{ij} is the friction coefficient, σ_{ij} is the noise amplitude, $\mathbf{v}_{ij} = \mathbf{v}_i - \mathbf{v}_j$, ζ_{ij} is a Gaussian random number with a zero mean and a unit variance that is chosen independently for each pair of interacting beads, and Δt is the time step.

Español and Warren[18] showed that the system samples the canonical ensemble and obeys the fluctuation−dissipation theorem (in the limit of $\Delta t \to 0$) if the following relations hold

$$\omega^{\mathrm{D}}(r_{ij}) = [\omega^{\mathrm{R}}(r_{ij})]^2 \tag{7}$$

$$\sigma_{ij}^{\,2} = 2\gamma_{ij}k_{\mathrm{B}}T \tag{8}$$

where T is the temperature and k_{B} is the Boltzmann constant. $\omega^{\mathrm{D}}(r_{ij})$ and $\omega^{\mathrm{R}}(r_{ij})$ are typically chosen[15] as

$$\omega^{\mathrm{D}}(r_{ij}) = [\omega^{\mathrm{R}}(r_{ij})]^2 = \begin{cases} \left(1-\frac{r_{ij}}{r_{\mathrm{c}}}\right)^2 & r_{ij} < r_{\mathrm{c}} \\ 0 & r_{ij} \geq r_{\mathrm{c}} \end{cases} \tag{9}$$

The evolution of DPD beads in time t is governed by Newton's equations of motion

$$\frac{\mathrm{d}\mathbf{r}_i}{\mathrm{d}t} = \mathbf{v}_i(t) \tag{10}$$

$$m_i\frac{\mathrm{d}\mathbf{v}_i}{\mathrm{d}t} = \mathbf{f}_i(t) = \sum_{i\neq j}(\mathbf{F}_{ij}^{\mathrm{C}} + \mathbf{F}_{ij}^{\mathrm{D}} + \mathbf{F}_{ij}^{\mathrm{R}})$$

Our mesoscale model of diblock copolymer $\mathrm{A}_n\mathrm{B}_m$ consists of A_n and B_m blocks connected end to end where n and m are the number of A and B beads, respectively. To determine the values of a_{ij}, we used expressions obtained by Groot and Warren that map DPD polymer models onto Flory−Huggins-type models.[15] Groot and Warren derived the following expressions for the like interactions

$$\frac{a_{\mathrm{AA}}r_{\mathrm{c}}}{k_{\mathrm{B}}T} \equiv \frac{a_{\mathrm{BB}}r_{\mathrm{c}}}{k_{\mathrm{B}}T} = \frac{75}{\rho {r_{\mathrm{c}}}^3} \tag{11}$$

and for the unlike interactions

$$\frac{a_{\mathrm{AB}}r_{\mathrm{c}}}{k_{\mathrm{B}}T} = \frac{a_{\mathrm{BB}}r_{\mathrm{c}}}{k_{\mathrm{B}}T} + a_1\left[1 + \frac{a_2}{(n+m)^{a_3}}\right]\chi_{\mathrm{AB}}^{\mathrm{eff}}(T) \tag{12}$$

where ρ is the bead number density, $\chi_{\mathrm{AB}}^{\mathrm{eff}}$ is the effective Flory−Huggins interaction parameter, and a_1, a_2, and a_3 are constants dependent on $\rho {r_{\mathrm{c}}}^3$ (e.g., $a_1 = 3.27$, $a_2 = 3.9$, and $a_3 = 0.51$ when $\rho {r_{\mathrm{c}}}^3 = 3$,[19] which is used in this work).

The confining walls are composed of four layers of DPD beads arranged on a face-centered-cubic lattice (following the work of Malfreyt and Tildesley[17]) with a wall density of approximately 3.5ρ. Although not presented here, the calculated A- and B-bead density profiles confirmed that the wall density used avoids the penetration of the diblock copolymer beads into the confining walls. For slits without nanopatterns, the opposing walls are either created from DPD beads of the same type, w_1, or created from DPD beads of different types, w_1 and w_2, which possess preferential affinity toward the B and A beads, respectively. For slits with nanopatterns, each wall contains alternating areas or strips created from w_1 and w_2 beads. Because the wall beads are tethered to their lattice positions by stiff harmonic springs, no additional repulsion interactions between the wall beads themselves are needed; therefore, we set $a_{w_1w_1} = a_{w_2w_2} = a_{w_1w_2} = 0$. Furthermore, for the sake of simplicity, the repulsion interactions between A and w_2 beads and between B and w_1 beads were considered to be the same as the like interactions for diblock copolymers (i.e., we set $a_{\mathrm{A}w_2} = a_{\mathrm{B}w_1} = a_{\mathrm{AA}} \equiv a_{\mathrm{BB}}$). Values of $a_{\mathrm{A}w_1}$ and $a_{\mathrm{B}w_2}$ were then varied in this study.

2.2. Computational Details. Throughout this article, we used the following reduced units; r_{c} is the unit of length, $k_{\mathrm{B}}T$ is the unit of energy, and the mass of a DPD bead is the unit of mass.

(15) Groot, R. D.; Warren, P. B. *J. Chem. Phys.* **1997**, *107*, 4423–4435.
(16) Kong, Y.; Manke, C. W.; Madden, W. G.; Schlijper, A. G. *Int. J. Thermophys.* **1994**, *15*, 1093–1101.
(17) Malfreyt, P.; Tildesley, D. J. *Langmuir* **2000**, *16*, 4732–4740.
(18) Español, P.; Warren, P. B. *Europhys. Lett.* **1995**, *30*, 191–196.
(19) Horsch, M. A.; Zhang, Z.; Iacovella, C. R.; Glotzer, S. C. *J. Chem. Phys.* **2004**, *121*, 11455–11462.

Using these reduced units, we set $\rho = 3$, $\sigma_{ij} = 3$, $K_w = 100$ and $\Delta t = 0.03$ and assumed that the DPD beads corresponding to the diblock copolymers and the walls have the same mass, m_{DPD}. We investigated the behavior of a symmetric diblock copolymer making up 10 DPD beads and consisting of 5 A and 5 B beads, A_5B_5, with $a_{AB} = 40$ (which corresponds to $\chi_{AB}^{eff} \simeq 2$), $K_s = 4$, and $r_0 = 0$. Groot and Madden[20] have shown that these values of K_s and r_0 provide a reasonable description of the structural properties of bulk diblock copolymer melts at $\rho = 3$. The lengths of the simulation box in the x and y directions were set to $L_x = L_y = 25$, and the slit width W was varied in the z direction from 2 to 20. In some cases, we also employed $L_x = 25$ and $L_y = 20$ to investigate finite-size and commensurate effects on the self-assembly, typically for cases near or at the phase boundaries between different types of nanostructures. Numerical integration of the DPD equations of motion (eq 10) was performed using the modified velocity Verlet algorithm.[15] To save CPU time, we implemented the cell list method for the energy and force calculations.[21,22] Typically, production runs spanned 600 000 time steps, but for some simulations near or at the phase boundaries between different types of nanostructures, as many as 2 000 000 time steps were used.

Simulations of the spontaneous formation of diblock copolymer nanostructures require us to employ a convenient simulation strategy that reasonably guarantees that the most stable structure will be found. In this work, we use the following strategy based on slow cooling of the diblock copolymer self-assembly.[19] The values of a_{AB} were slowly increased from $a_{AB} = 25$ to the target value of 40, whereby because $\chi_{AB}^{eff} \propto 1/T$[23] this approach corresponds to a slow decrease in T. Each increase in a_{AB} was followed by a DPD simulation run that allowed the system to relax to an equilibrated state. The increase in a_{AB} was typically performed with steps equal to unity and with a relaxation period of 60 000 time steps.

In addition to evaluating thermodynamic properties such as the interparticle energy, the pressure tensor (obtained using the Irvin−Kirkwood definition), the temperature, and A- and B-bead density profiles across the slit, we also evaluated the following structural properties of the diblock copolymers to deduce their conformational behavior in confinement.

The mean square end-to-end distance

$$R_e^2 = \left\langle \frac{1}{N}\sum_{i=1}^{N} (\mathbf{r}_{1,i} - \mathbf{r}_{n+m,i})^2 \right\rangle \quad (13)$$

and the mean square radius of gyration

$$R_g^2 = \left\langle \frac{1}{N}\sum_{i=1}^{N} \left[\frac{1}{n+m}\sum_{j=1}^{n+m} (\mathbf{r}_{j,i} - \mathbf{r}_{com,i})^2 \right] \right\rangle \quad (14)$$

are typically used to define the characteristic size of a polymer chain. In eqs 13 and 14, N is the number of diblock copolymers, $\mathbf{r}_{j,i}$ is the position of bead j belonging to diblock copolymer i, $\mathbf{r}_{com,i}$ is the position of the center-of-mass of diblock copolymer i, and $\langle . \rangle$ denotes an ensemble average. Polymer chains confined in planar slits can be further characterized by the mean square radius-of-gyration parallel and perpendicular to the wall, $R_{g,\parallel}^2$ and $R_{g,\perp}^2$, respectively, which are given by the expressions

$$R_{g,\parallel}^2 = \left\langle \frac{1}{N}\sum_{i=1}^{N} \left\{ \frac{1}{n+m}\sum_{j=1}^{n+m} [(x_{j,i} - x_{com,i})^2 + (y_{j,i} - y_{com,i})^2] \right\} \right\rangle \quad (15)$$

$$R_{g,\perp}^2 = \left\langle \frac{1}{N}\sum_{i=1}^{N} \left[\frac{1}{n+m}\sum_{j=1}^{n+m} (z_{i,j} - z_{com,i})^2 \right] \right\rangle$$

where x, y, and z are the Cartesian coordinates of $\mathbf{r}$. Note that $R_g^2 = R_{g,\parallel}^2 + R_{g,\perp}^2$.

Finally, the nematic order parameter

$$P_{2,d} = \frac{3}{2}\langle \lambda_{max} \rangle \quad (16)$$

is a convenient measure of orientational order,[24] which we calculated in this study. In eq 16, λ_{max} is the largest eigenvalue of the Saupe tensor

$$Q_{\alpha\beta} = \frac{1}{N}\sum_{i=1}^{N} e_{i,\alpha} e_{i,\beta} - \frac{\delta_{\alpha\beta}}{3} \quad (17)$$

where e_i is the unit vector along the end-to-end direction of diblock copolymer i and $\delta_{\alpha\beta}$ is the Kronecker delta. $P_{2,d}$ is zero in a completely orientationally disordered state and is unity if the diblock copolymers are perfectly aligned.

3. Results and Discussion

We carried out DPD simulations of the self-assembly of the A_5B_5 copolymers in planar slits with and without nanopatterns. Knowledge of the self-assembly in slits without nanopatterns provides a means of rationalizing the self-assembly in the nanopatterned slits. We were particularly interested in determining whether the self-assembly behavior in the slits with no nanopatterns could be superimposed to predict the self-assembly behavior accurately in the various nanopattern scenarios. Such predictive capability would be a powerful tool in the rational systematic design of nanostructures and nanostructure templates.

In this study, we varied the slit width W from 2 to 20 with a unit step and varied the DPD repulsion parameters a_{Aw_1} and a_{Bw_2} typically from the value of $a_{AA} \equiv a_{BB}$ to the value of a_{AB} (i.e., from 25 to 40). Ratios of $\Delta a_{Aw_1}/\Delta a_{AB}$ and $\Delta a_{Bw_2}/\Delta a_{AB}$, where $\Delta a_{Aw_1} = a_{Aw_1} - a_{AA}$, $\Delta a_{Bw_2} = a_{Bw_2} - a_{AA}$, and $\Delta a_{AB} = a_{AB} - a_{AA}$, were used to characterize the phobicity of the A and B beads toward the w_1- and w_2-wall beads, respectively. The phobicity increases with increasing values of $\Delta a_{Aw_1}/\Delta a_{AB}$ or analogously $\Delta a_{Bw_2}/\Delta a_{AB}$. Note that $\Delta a_{Aw_2} = \Delta a_{Bw_1} = 0$ for our chosen parameter set given in section 2.1.

3.1. Planar Slits without Nanopatterns. We first studied the self-assembly of A_5B_5 copolymers confined between planar walls where the opposing walls are (a) both composed of w_1-wall beads (referred to hereafter as w_1 walls) and (b) composed of different types of wall beads, w_1 wall and w_2 wall, respectively (referred to hereafter as w_1 and w_2 walls).

3.1.1. Planar Slits with w_1 Walls. We studied systems with repulsion parameters $\Delta a_{Aw_1}/\Delta a_{AB} = \{0, {}^1/_3, {}^2/_3, 1, {}^4/_3\}$ where for all of these systems, except the first listed, B beads have a preferential affinity for w_1-wall beads because $\Delta a_{Bw_1} = 0$. Figure 2 displays an $a_{Aw_1} - W$ phase diagram for the A_5B_5 system, where the particular phases were determined by an analysis of both the

(20) Groot, R. D.; Madden, T. J. *J. Chem. Phys.* **1998**, *108*, 8713–8724.
(21) Frenkel, D.; Smit, B. *Understanding Molecular Simulation: From Algorithms to Applications*, 2nd ed.; Academic Press: London, 2002.
(22) Allen, M. P.; Tildesley, D. J. *Computer Simulation of Liquids*, 2nd ed.; Clarendon Press: Oxford, U.K., 1987.
(23) Flory, P. J. *Principles of Polymer Chemistry*, 3rd ed.; Cornell University Press: New York, 1953.
(24) De Gennes, P. G.; Prost, J. *The Physics of Liquid Crystals*; Clarendon Press: Oxford, U.K., 1993.

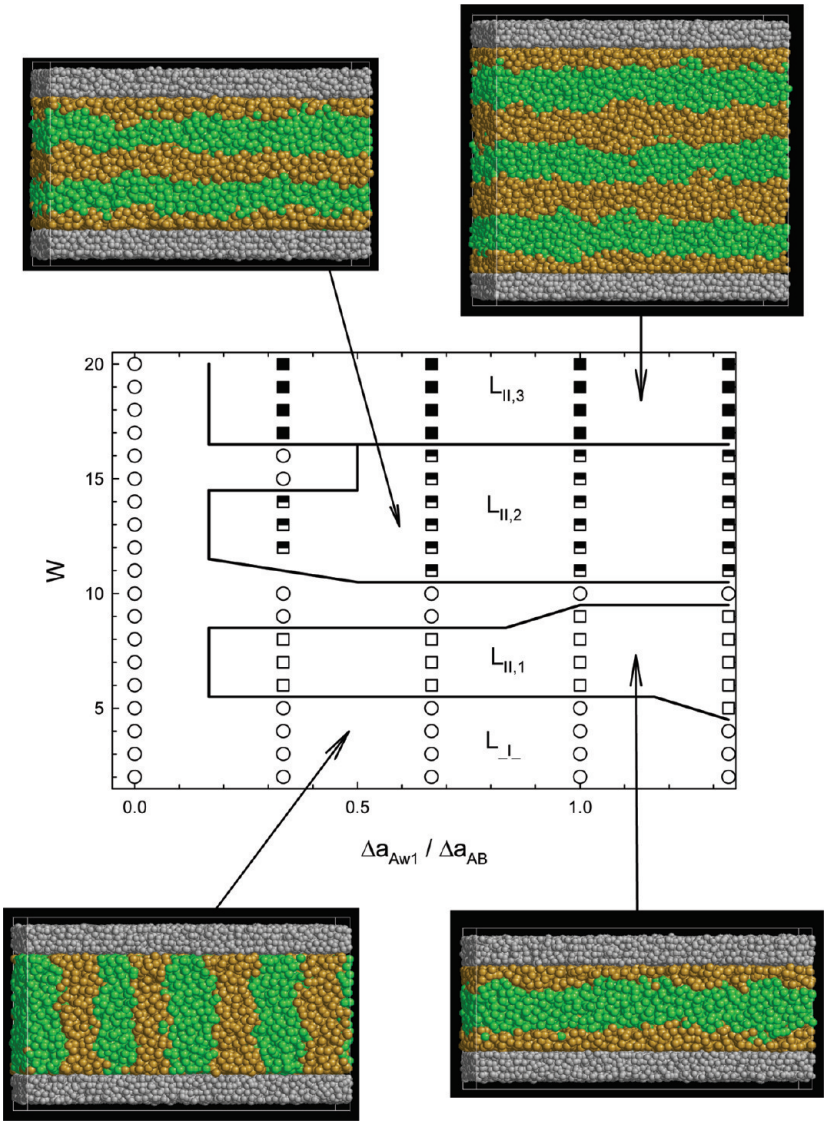

Figure 2. Phase diagram of the A_5B_5 system confined in planar slits with w_1 walls, together with examples of simulation configurations for the particular lamellar phases. W is the slit width, and $\Delta a_{Aw_1}/\Delta a_{AB}$ is a measure of the phobicity of the A beads toward the w_1-wall beads; B beads have preferentially affinity toward the w_1-wall beads ($\Delta a_{Bw_1}/\Delta a_{AB} = 0$). Symbols represent simulation results, and solid lines indicate approximate microphase separation boundaries. The symbols refer to a perpendicular lamellar phase ($L_\perp$) and parallel lamellar phases with ν A lamellae ($L_{\parallel,\nu}$). Green and gold spheres represent A and B beads, respectively, and gray spheres represent wall beads.

isosurfaces and the A- and B-bead density profiles across the slit, together with a visual inspection of the equilibrium configurations. For narrow slit widths up to 4 or 5, the system forms a perpendicular lamellar phase (denoted as $L_\perp$) regardless of the interaction strength between the chains and the walls for steric reasons (i.e., the slit widths are simply too narrow to accommodate parallel lamellae). Figure 2 also shows that when no preferential affinity of the A or B beads toward the wall beads exists (i.e., $\Delta a_{Aw_1}/\Delta a_{AB} = 0$) the system self-assembles into a perpendicular lamellar phase for all slit widths. For these cases, perpendicular alignment is preferred over parallel alignment because the wall-diblock copolymer adsorption energy does not play a significant role; moreover, the perpendicular alignment allows the system to adopt its preferred bulk lamellae spacing. Figure 2 further shows that with increasing $\Delta a_{Aw_1}/\Delta a_{AB}$ (i.e., phobicity of the A beads toward the w_1-wall beads) the systems at $W > 5$ prefer to form parallel lamellar phases spontaneously with ν lamellae (denoted as $L_{\parallel,\nu}$) as a result of the more favorable wall−diblock copolymer adsorption energy for parallel alignment with respect to perpendicular alignment, which is a consequence of the preferential adsorption of the B beads. (Note that throughout this article ν refers to the number of A lamellae unless indicated otherwise; for example, in Figure 1a, $\nu = 2$.) The lamellae adopts a perpendicular alignment only when the system becomes very structurally frustrated between the $L_{\parallel,\nu}$ and $L_{\parallel,\nu+1}$ orientations. In such cases, the slit width does not correspond to either the ν or the $\nu + 1$ lamellae spacing. For strong phobicity between the A beads and wall ($\Delta a_{Aw_1}/\Delta a_{AB} > 0.85$), $L_\perp$ is formed only between $L_{\parallel,1}$ and $L_{\parallel,2}$.

Figures 3 and 4 show R_e^2, R_g^2, and $P_{2,d}$ as a function of W for two particular values of phobicity, $\Delta a_{Aw_1}/\Delta a_{AB} = 0$ and $\Delta a_{Aw_1}/\Delta a_{AB} = 1$, which provide further insight into the behavior of the diblock copolymer self-assembly. For $\Delta a_{Aw_1}/\Delta a_{AB} = 0$, where the system forms only perpendicular lamellae, the diblock copolymers become increasingly elongated in the perpendicular direction and the system loses orientational order (i.e., $P_{2,d}$ decreases) as W increases up to about 6. Because the chains in this case have no preferential interactions with the walls, this behavior can be attributed only to a release of the steric constraint imposed by the

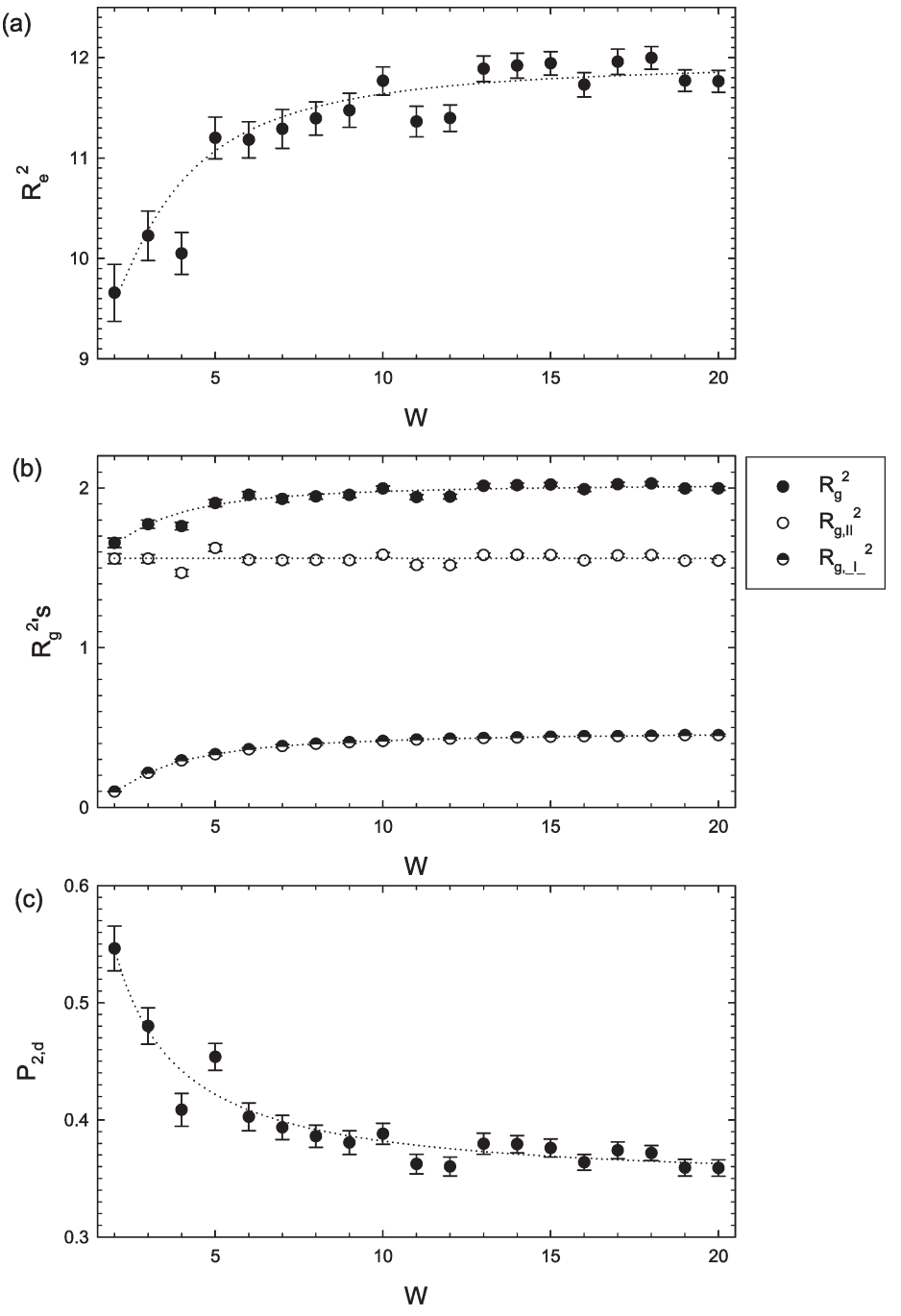

Figure 3. (a) Mean square end-to-end distance, R_e^2, (b) mean square radius-of-gyration, R_g^2, and (c) nematic order parameter, $P_{2,d}$, as a function of the slit width, W, for the A_5B_5 copolymers confined in planar slits with w_1 walls, where $\Delta a_{Aw_1}/\Delta a_{AB} = \Delta a_{Bw_1}/\Delta a_{AB} = 0$. Symbols represent simulation results, where dotted lines are drawn as a guide to the eye.

confining walls. Above $W \approx 6$, the size of the copolymers and the system orientational order is only marginally affected by W.

Very different conformational behavior for the diblock copolymers is seen for $\Delta a_{Aw_1}/\Delta a_{AB} = 1$ in Figure 4, where the system self-assembles into both parallel and perpendicular alignments depending on W. For $W < 6$, where the systems exhibit perpendicular alignment, R_e^2, R_g^2, and $P_{2,d}$ exhibit similar trends as in the case of $\Delta a_{Aw_1}/\Delta a_{AB} = 0$ (i.e., the diblock copolymers elongate in the perpendicular direction and the system orientational order decreases). For $W \geq 6$, the transformation into a particular parallel phase is accompanied by a dramatic elongation of the diblock copolymers in the perpendicular direction, as evidenced by the increase in R_e^2, $R_{g,\perp}^2$, and $P_{2,d}$ with increasing W within each $L_{||,\nu}$ phase. As the slit width is increased, structural frustration of the diblock copolymers in the parallel lamellae is relieved by either the formation of an additional parallel lamellae or, in the case where $W \simeq 10$, a reorientation of the parallel lamellae to perpendicular lamellae. For either of these occurrences, the diblock copolymers have collapsed upon themselves to minimize the free energy while subsequently losing orientational order. Note that for $W > 6$, $R_{g||}^2$ adopts distinct values for $L_\perp$ and $L_{||,\nu}$ and they do not depend on W within the perpendicular and parallel lamellar regions. For the other nonzero values of $\Delta a_{Aw_1}/\Delta a_{AB}$ shown in Figure 2, we observed similar dramatic differences in the conformational behavior when compared to $\Delta a_{Aw_1}/\Delta a_{AB} = 0$, but they are not shown here.

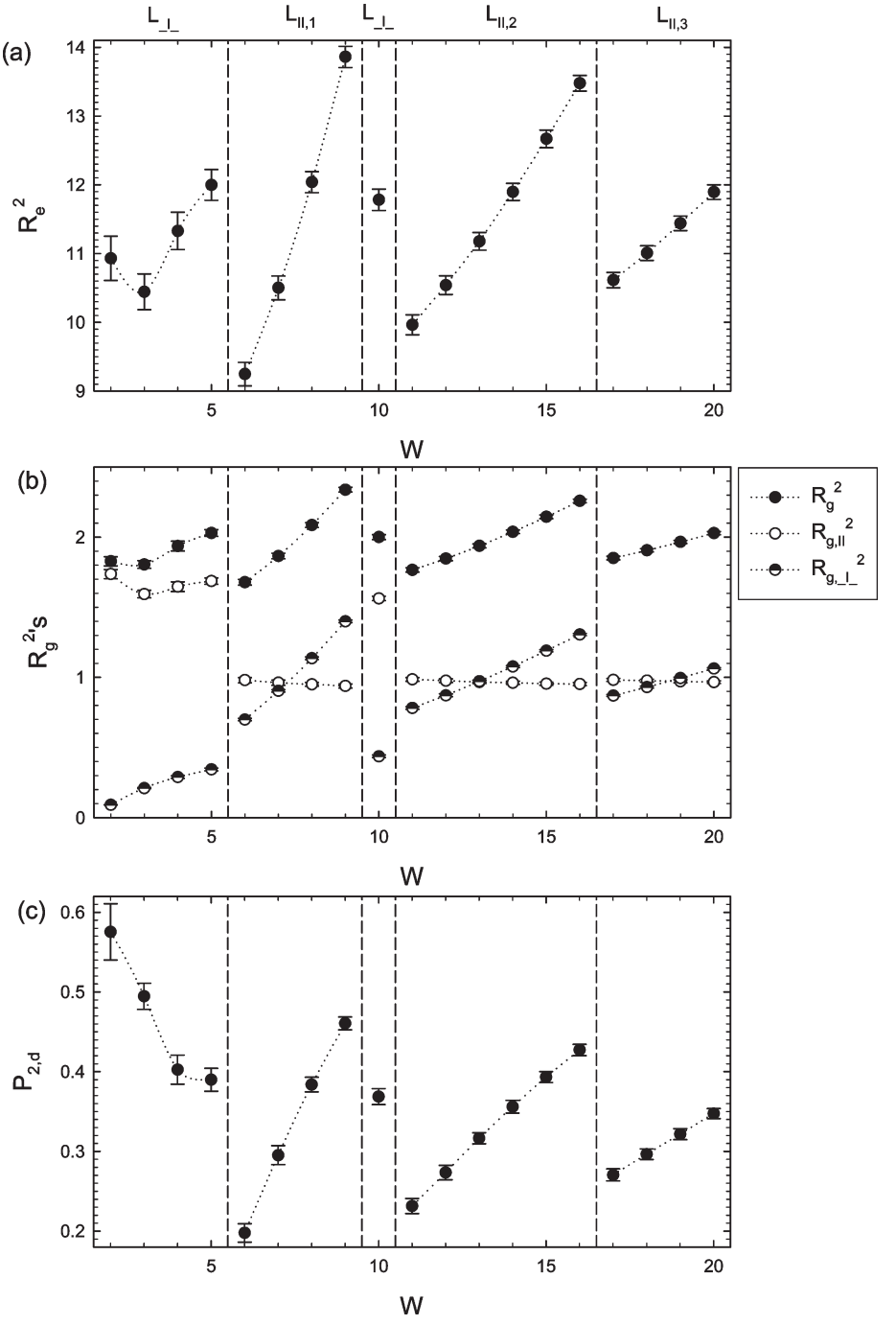

Figure 4. (a) Mean square end-to-end distance, R_e^2, (b) mean square radius of gyration, R_g^2, and (c) nematic order parameter, $P_{2,d}$, as a function of the slit width, W, for the A_5B_5 copolymers confined in planar slits with w_1 walls, where $\Delta a_{Aw_1}/\Delta a_{AB} = 1$ and $\Delta a_{Bw_1}/\Delta a_{AB} = 0$. Symbols represent simulation results where dotted lines are drawn as a guide to the eye and vertical dashed lines mark approximate microphase separation boundaries. Symbols for particular phases are the same as in Figure 2.

The conformational behavior exhibited in Figures 3 and 4 correlates with the dependence of the lamellae width, W_{LAM}, on W as shown in Figure 5, where the values of W_{LAM} were determined by Voronoi tessellation.[25] Note that for $W < 6$, perpendicular lamellae are quite irregular and therefore the value of W_{LAM} cannot be reliably determined. As expected for $\Delta a_{Aw_1}/\Delta a_{AB} = 0$, the lamellar width does not depend on W and the values of W_{LAM} correspond to the natural lamellar width in the bulk. For $\Delta a_{Aw_1}/\Delta a_{AB} = 1$, the lamellar widths increase with increasing W within each parallel lamellar region of the phase diagram coinciding with the elongation of the chains in the perpendicular direction and the increase in orientational order exhibited in Figures 3 and 4. For the parallel lamellae phases only, Figure 5b also displays the thickness of the adsorbed B-bead layer, W_L, where the values of W_L were evaluated to be $W_L = {}^1/_2[W - (2\nu - 1)W_{LAM}]$. Similar to the behavior found for the lamella thickness, we see that with increasing slit width the adsorbed layer thickness increases within each parallel lamellar region, however in a less dramatic manner. In addition, the adsorbed layer thickness becomes less dependent on the slit width

(25) Arya, S.; Malamatos, T.; Mount, D. M. *Space-Efficient Approximate Voronoi Diagrams*; Proceedings of the 34th ACM Symposium on Theory of Computing; STOC, Monreal, Canada, 2002; pp 721−730.

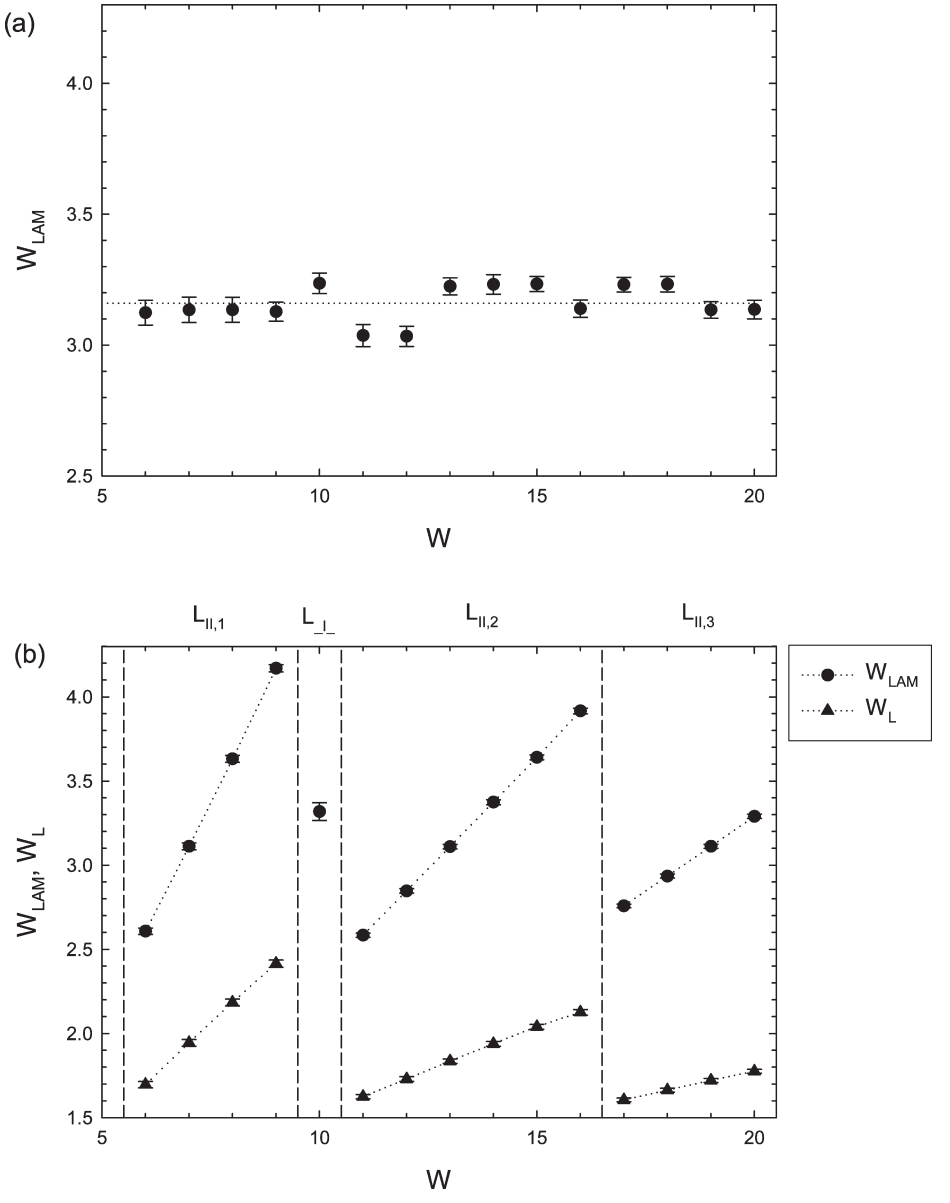

Figure 5. Lamella width, W_{LAM}, and thickness of the adsorbed layer, W_L, as a function of the slit width, W, for the A_5B_5 copolymers confined in planar slits with w_1 walls, where (a) $\Delta a_{Aw_1}/\Delta a_{AB} = \Delta a_{Bw_1}/\Delta a_{AB} = 0$ and (b) $\Delta a_{Aw_1}/\Delta a_{AB} = 1$ and $\Delta a_{Bw_1}/\Delta a_{AB} = 0$. Symbols represent simulation results, where dotted lines are drawn as a guide to the eye and vertical dashed lines mark approximate microphase separation boundaries. Symbols for particular phases are the same as in Figure 2.

when more lamellae are present in the system. This behavior can be attributed to the decreasing influence of the wall interactions because as the slit width increases, the system is approaching bulk-phase behavior.

3.1.2. Planar Slits with w_1 and w_2 Walls. Figure 6 presents an $a_{Bw_2}-W$ phase diagram for the confined A_5B_5 copolymers, where the A beads interact with the w_1 walls by $\Delta a_{Aw_1}/\Delta a_{AB} = 1$ and the B$-w_2$ repulsion interaction is varied as $\Delta a_{Bw_2}/\Delta a_{AB} = \{0, {}^1/_2, 1\}$. Here, A and B beads have preferential affinity for the w_2- and w_1-wall beads, respectively, because $\Delta a_{Aw_2} = \Delta a_{Bw_1} = 0$. As in the previous case where the opposing walls were identical, for very narrow slit widths of up to 2 or 3 the system self-assembles into perpendicular alignment regardless of the strength of the interaction between the diblock copolymers and the walls. For narrow slit widths between 3(4) and 5, the system forms only A and B adsorbed layers, which we denote as an adsorbed-layer phase, L. As another similarity to the previous case, a variety of parallel alignments are formed at larger slit widths. However, the system displays two distinguishable phases with parallel alignment: parallel lamellar phases with B-adsorbed layers on both confining walls (as in the previous case) and parallel lamellar phases with A- and B-layers adsorbed onto the w_2 and w_1 walls, respectively, with the latter phases termed adsorbed layer−parallel lamellar phases and denoted as L−$L_{\parallel,\nu}$. In our simulations, L−$L_{\parallel,\nu}$ phases exist for $\Delta a_{Bw_2}/\Delta a_{AB} < 1$, where B beads can also adsorb onto the w_2 wall because of the lower B-wall phobicity with respect to the A-wall phobicity (i.e., due to $\Delta a_{Bw_2} < \Delta a_{Aw_1}$). For $\Delta a_{Bw_2}/\Delta a_{AB} = 0$, L and L−$L_{\parallel,\nu}$ phases always precede $L_{\parallel,\nu}$ and $L_{\parallel,\nu+1}$ phases, respectively. However, for $\Delta a_{Bw_2}/\Delta a_{AB} = 0.5$, we see the disappearance of $L_{\parallel,2}$ and $L_{\parallel,3}$ phases, along with the formation of $L_\perp$ between L and $L_{\parallel,1}$, and a mixed lamellar phase ($L_{\perp+\parallel}$) between L−$L_{\parallel,1}$ and L−$L_{\parallel,2}$. For all slit widths, the system with $\Delta a_{Bw_2}/\Delta a_{AB} = \Delta a_{Aw_1}/\Delta a_{AB} = 1$ does not exhibit $L_{\parallel,\nu}$ (as expected from the symmetry in the diblock copolymer−wall interactions) and displays a succession of $L_\perp$/L/$L_\perp$/L−$L_{\parallel,1}$/L−$L_{\parallel,2}$/L−$L_{\parallel,3}$ phases. Note that we have verified the stability of the perpendicularly aligned phases

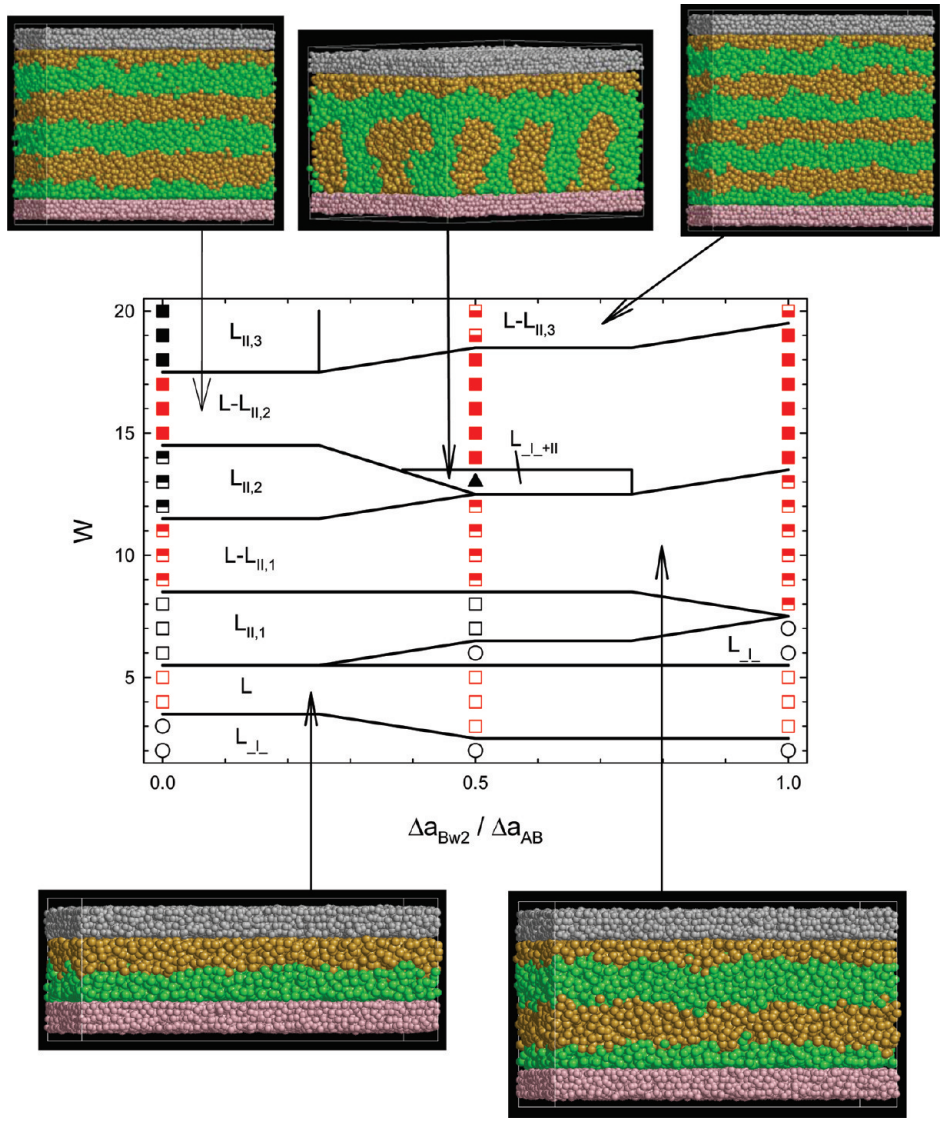

Figure 6. Phase diagram of the A_5B_5 system confined in planar slits with w_1 and w_2 walls, where $\Delta a_{Aw_1}/\Delta a_{AB} = 1$ and $\Delta a_{Bw_2}/\Delta a_{AB}$ varies. Also shown are examples of simulation configurations for the layer, layer−parallel lamellar, and mixed lamellar phases; simulation configurations for the perpendicular and parallel lamellar phases are analogous to those shown in Figure 2. W is the slit width, and $\Delta a_{Aw_1}/\Delta a_{AB}$ and $\Delta a_{Bw_2}/\Delta a_{AB}$ are measures of the phobicity of the A and B beads toward the w_1- and w_2-wall beads, respectively. Symbols represent simulation results, and solid lines mark approximate phase boundaries. Symbols refer to a perpendicular lamellar phase ($L_\perp$), a mixed lamellar phase ($L_{\perp+\parallel}$), parallel lamellar phases with ν A lamellae ($L_{\parallel,\nu}$), a layer phase (L), and layer−parallel lamellar phases with ν A lamellae ($L-L_{\parallel,\nu}$). Green and gold spheres represent A and B beads, respectively, and gray and pink spheres represent w_1- and w_2-wall beads, respectively.

for $W > 5$ and the mixed lamellar phase $L_{\perp+\parallel}$ by performing DPD simulations with box lengths of $L_x = 25$ and $L_y = 20$.

As an example of the conformational behavior of the systems shown in Figure 6, R_e^2, R_g^2, and $P_{2,d}$ are shown in Figure 7 for $\Delta a_{Bw_2}/\Delta a_{AB} = 0$. Similar to the behavior exhibited in planar slits with w_1 walls when $\Delta a_{Aw_1}/\Delta a_{AB} = 1$ and $\Delta a_{Bw_1}/\Delta a_{AB} = 0$, the succession of $L/L_{\parallel,1}/L-L_{\parallel,1}/L_{\parallel,2}/L-L_{\parallel,2}/L_{\parallel,3}$ phases is accompanied by the elongation of the diblock copolymers in the perpendicular direction and an increase in the system orientational order within each phase for $W > 3$. The stretching and increasing orientational order is then relieved by the transformation of one phase into another as W increases. Similar trends in the conformational behavior as depicted by R_e^2, R_g^2, and $P_{2,d}$ are also exhibited for $\Delta a_{Bw_2}/\Delta a_{AB} > 0$ (not shown here).

3.2. Nanopatterned Planar Slits. Next, we study the self-assembly of A_5B_5 copolymers confined in nanopatterned planar slits for three mutual locations of the nanopatterns and for two differently sized nanopatterned strips: $L_{NP} = 12.5$ and 6.25, as depicted in Figure 8. In Figure 8, opposing walls have strips composed of w_1- and w_2-wall beads that are vertically (a) aligned, (b) staggered, and (c) partially staggered. After setting the A-bead repulsion parameters to $\Delta a_{Aw_1}/\Delta a_{AB} = 1$ and $\Delta a_{Aw_2} = \Delta a_{Bw_1} = 0$, we studied systems for B-bead repulsion parameters $\Delta a_{Bw_2}/\Delta a_{AB} = \{0, {}^1/_2, 1\}$.

In Figure 8, the nanopatterns on opposing walls can be partitioned such that they correspond to the planar surfaces without nanopatterns investigated previously and are indicated as such by the red dashed lines. Hence, it is reasonable to attempt to rationalize the self-assembly of the A_5B_5 copolymers in the nanopatterned planar slits on the basis of the behavior observed in the planar slits without nanopatterns. In particular, we investigate the applicability of superimposing the observed nanostructures in planar slits without nanopatterns to predict the nanostructures formed when nanopatterns are present.

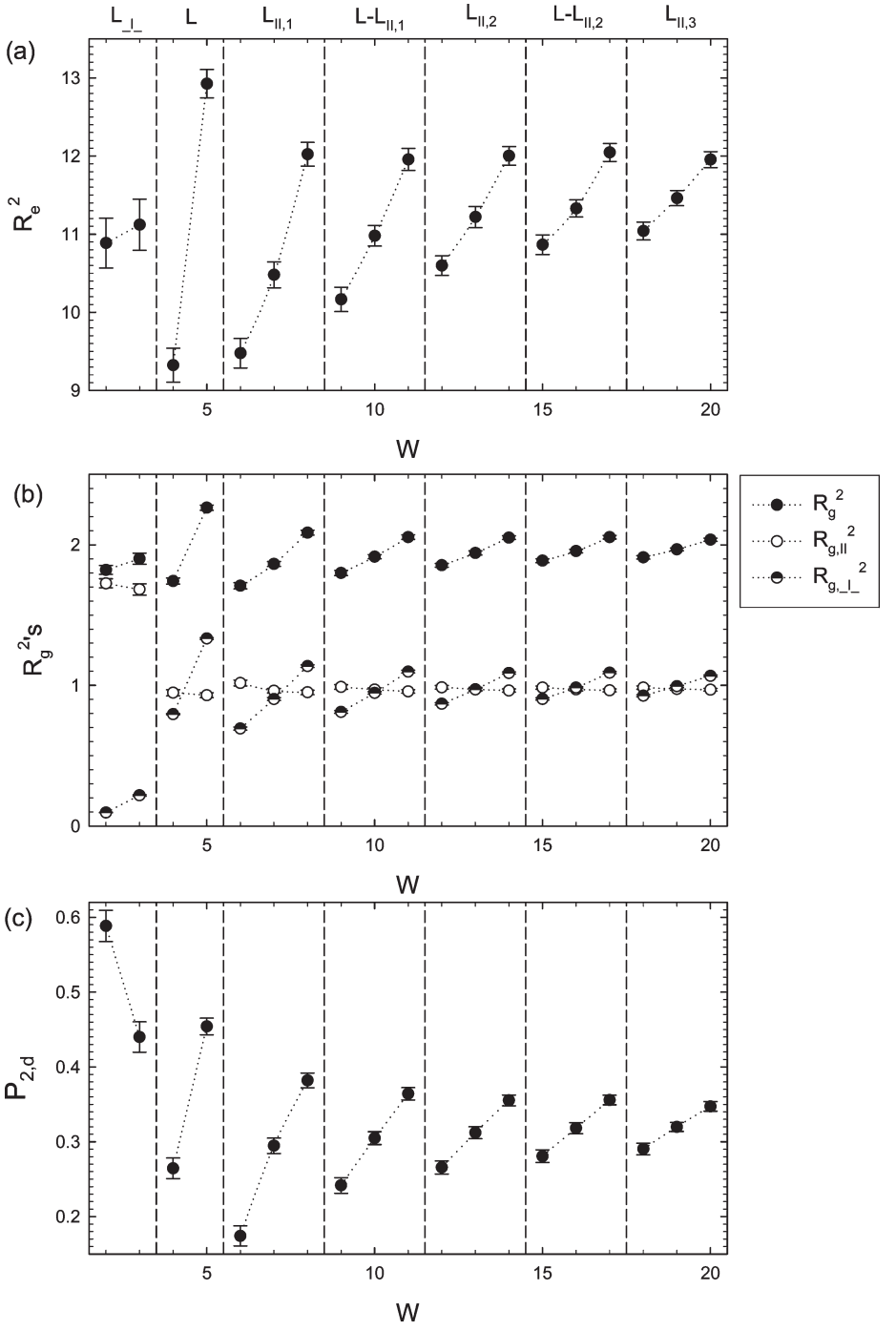

Figure 7. (a) Mean square end-to-end distance, R_e^2, (b) mean square radius of gyration, R_g^2, and (c) nematic order parameter, $P_{2,d}$, as a function of the slit width, W, for the A_5B_5 copolymers confined in planar slits with w_1 and w_2 walls and with $\Delta a_{Aw_1}/\Delta a_{AB} = 1$ and $\Delta a_{Bw_2}/\Delta a_{AB} = 0$. Symbols represent simulation results where dotted lines are drawn as a guide to the eye and vertical dashed lines mark approximate microphase separation boundaries. Symbols for particular phases are the same as in Figure 6.

Corresponding to the partitions indicated in Figure 8, the superposition description is satisfied if the nanostructure in the nanopatterned slit can be approximated by a collective sequence of previously determined nanostructures. Our attempt to depict a phase diagram via such a superposition description is performed in the following manner. For each slit width, B-w_2 phobicity pair in the phase diagram, we first provide a schematic indicating the type of nanostructure observed in the planar slits without nanopatterns that corresponds to each of the partitions. If a nanostructure for a particular $W-\Delta a_{Bw_2}$ pair corresponds to simply superimposing the nanostructures observed in planar slits without nanopatterns, then we provide an equilibrium configuration snapshot (exceptions are for previously shown configurations such as $L_\perp$ or $L_{\parallel,\nu}$). Otherwise, a cross is placed over the schematic of the nanostructure(s) corresponding to the case without nanopatterns, whereas next to this schematic we indicate the actual nanostructure that is formed. In other words, in the phase diagram, the schematics of nanostructures that have a cross through them do not follow from superimposing the analogous nanostructures formed by the self-assembly in planar slits without nanopatterns.

As a further explanation of constructing the schematics that are used to depict the phase behavior, Figure 9 provides three

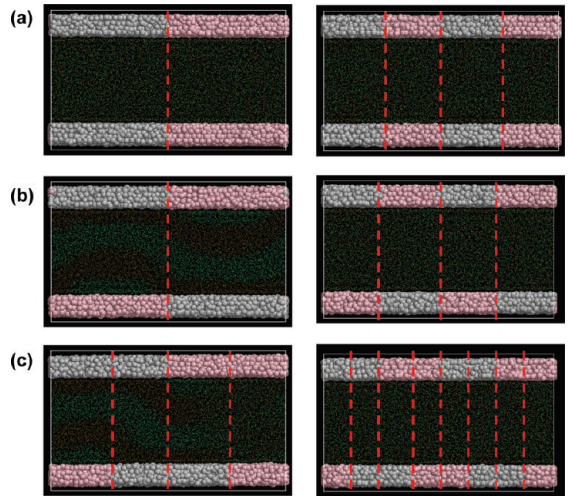

Figure 8. Nanopatterned planar slits, where the nanopatterns on opposing surfaces are vertically (a) aligned, (b) staggered, and (c) partially staggered. Left and right columns correspond to the nanopatterned planar slits with wide (L_{NP} = 12.5) and narrow (L_{NP} = 6.25) strips, respectively. Red dashed lines indicate virtual partitioning of the nanopatterned slits into portions corresponding to the planar slits without nanopatterns (i.e., planar slits with w_1 walls and planar slits with w_1 and w_2 walls). Gray and pink spheres represent w_1- and w_2-wall beads, respectively.

examples of some nanostructures that are observed in planar slits with wide, vertically aligned nanopatternes. In the first example where W = 7 (Figure 9a), the schematic indicates the formation of $L_{\parallel,1}$ and $L_{\perp}$ in the w_1 and w_2 portions of the nanopatterned planar slit, respectively. The total phase behavior in the nanopatterned planar slit can be predicted by superimposing the $L_{\parallel,1}$ and $L_{\perp}$ nanostructures observed in planar slits without nanopatterns, more precisely, in planar slits of W = 7 that exhibit $L_{\perp}$ and $L_{\parallel,1}$ phases for 0 and 1 block-wall phobicities, respectively, as shown in Figure 2. In the second example where W = 20 (Figure 9b), the schematic indicates that the superposition description is not valid because instead of the formation of $L_{\parallel,3}$ and $L_{\perp}$ phases in the w_1 and w_2 portions of the nanopatterned planar slit, respectively, the system exhibits $L_{\parallel,3}$ behavior only. Therefore, in this particular case, the nanopatterned system only partially follows the superposition description, where a cross overlays the part of the schematic corresponding to $L_{\perp}$. In the third example where W = 11 (Figure 9c), the behavior observed in the planar slits without nanopatterns would suggest self-assembly into an $L_{\parallel,2}$ phase and an inverse $L_{\parallel,2}$ phase (indicated by $L_{\parallel,2}^{-1}$) in the w_1 and w_2 portions of the nanopatterned planar slits, respectively, but instead the system self-assembles into only an $L_{\perp}$ phase. (In an $L_{\parallel,\nu}^{-1}$ phase, the roles of the A and B beads are interchanged, where now the A beads exhibit preferential affinity toward the walls and lamellae are formed by B beads (and correspondingly ν refers to the number of B lamellae).) Here, the system does not follow the superposition description in either the w_1 or the w_2 portion of the nanopatterned planar slit, thus both parts of the schematic are crossed out.

As performed for planar slits without nanopatterns, in addition to DPD simulations with box lengths of $L_x = L_y$ = 25, we also investigated finite-size and commensurate effects by performing additional DPD simulations with L_x = 25 and L_y = 20. In most cases, these simulations confirmed our findings from the original-size simulations, except for a few cases near the microphase-separation boundaries. In such cases, we indicate both self-assembled nanostructures in the phase diagrams. A determination

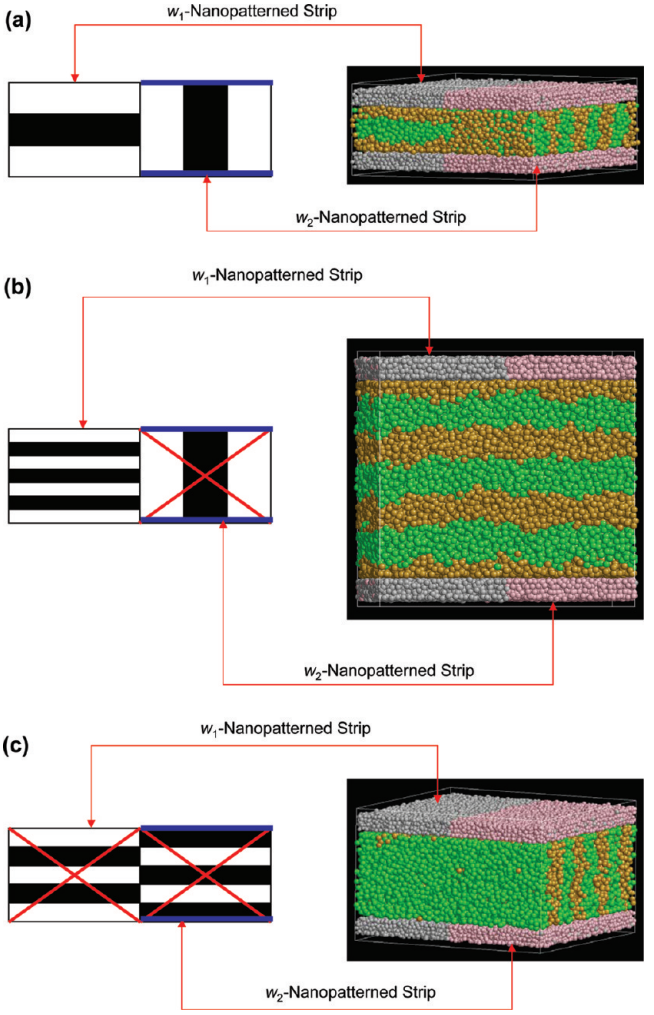

Figure 9. Examples of the approach used to construct the schematic phase diagrams of A_5B_5 copolymers confined in planar slits with wide, vertically aligned nanopatterns. In portions a and b, B beads have preferential affinity toward w_1 strips and neither A nor B beads have preferential affinity toward w_2 strips. In portion c, A and B beads have preferential affinity toward w_2 and w_1 strips, respectively. The left column shows examples of the schematics that are reported in the phase diagram, whereas the right column shows the observed phase behavior via a simulation configuration. Each schematic consists of two parts corresponding to w_1 and w_2 portions of the nanopatterned slits, where for each partition the lamellar phase found in the corresponding planar slit without nanopatterns is displayed. Crosses through a partition of the schematic indicate that this phase is not present in the actual nanopatterned planar slit and thus a superposition description is not valid. Green and gold spheres represent A and B beads, respectively, and gray and pink spheres represent w_1 and w_2 wall beads, respectively.

of the true nanostructures very near these microphase separation boundaries would require a systematic analysis of finite-size and commensurate effects accompanied by free-energy calculations,[26] which is beyond the scope of this work.

3.2.1. Planar Slits with Wide, Vertically-Aligned Nanopatterns. Figure 10 presents the phase behavior of A_5B_5 copolymers confined in planar slits with wide (L_{NP} = 12.5), vertically aligned nanopatterns in a schematic manner for the various pairs of W and $\Delta a_{Bw_2}/\Delta a_{AB}$ studied. Figure 11 provides simulation config-

(26) Martínez-Veracoeche, F. J.; Escobedo, F. A. *J. Chem. Phys.* **2006**, *125*, 104907.

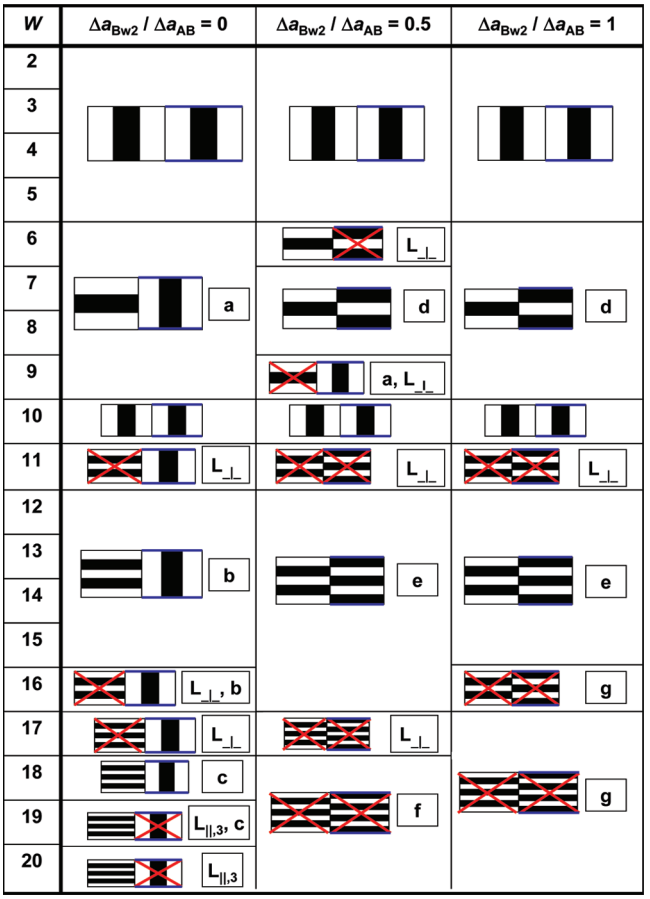

Figure 10. Self-assembly of the A_5B_5 systems confined in nanopatterned planar slits, where strips on opposing surfaces are vertically aligned with size $L_{NP} = 12.5$. W is the slit width, and $\Delta a_{Bw_2}/\Delta a_{AB}$ is a measure of the phobicity of the B blocks toward the w_2 walls. Schematics indicate the lamellar alignment in the planar slits without nanopatterns (i.e., in the planar slits with w_1 walls). w_1 and w_2 walls are represented by black and blue lines, respectively. Crosses indicate cases where nanostructures did not result from the superposition of the lamellar alignment in the underlying planar slits without nanopatterns. Letters a−g represent simulation configurations for some select nanostructures formed in the nanopatterned planar slits, which are shown in Figure 11. Other legend definitions are $L_\perp$, a perpendicular lamellar phase, and $L_{\parallel,3}$, a parallel lamellar phase with three A lamellae. For cases in which different nanostructures were observed for differently sized simulation cells, both nanostructures are shown, separated by a comma.

urations for some of the nanostructures formed, which correspond to the letters given in Figure 10. A few interesting features of Figure 10 are worth noting. Overall, the resulting nanostructures follow from the superposition of the lamellar alignment observed in the planar slits without nanopatterns (i.e., in the planar slits with w_1 walls), with an exception for wide slit widths, $W > 15$. For narrow slit widths of up to 5, the system follows superposition behavior, where $L_\perp$ phases are formed regardless of the value of $\Delta a_{Bw_2}/\Delta a_{AB}$. Considering all slit widths for the $\Delta a_{Bw_2}/\Delta a_{AB} = 0$ case, we observed the formation of nanostructures given by the superposition behavior of the $L_{\parallel,\nu}$ and $L_\perp$ phases in all cases (denoted as $L_{\parallel,\nu} + L_\perp$, where configuration snapshots are shown in Figure 11a−c), with the exception of the relaxation of the system into $L_\perp$ phases between $L_{\parallel,1} + L_\perp$ and $L_{\parallel,2} + L_\perp$ and between $L_{\parallel,2} + L_\perp$ and $L_{\parallel,3} + L_\perp$ phases. The observed interface morphology between parallel and perpendicular lamellar domains is known as Schrek's surface twist boundary. Schrek's

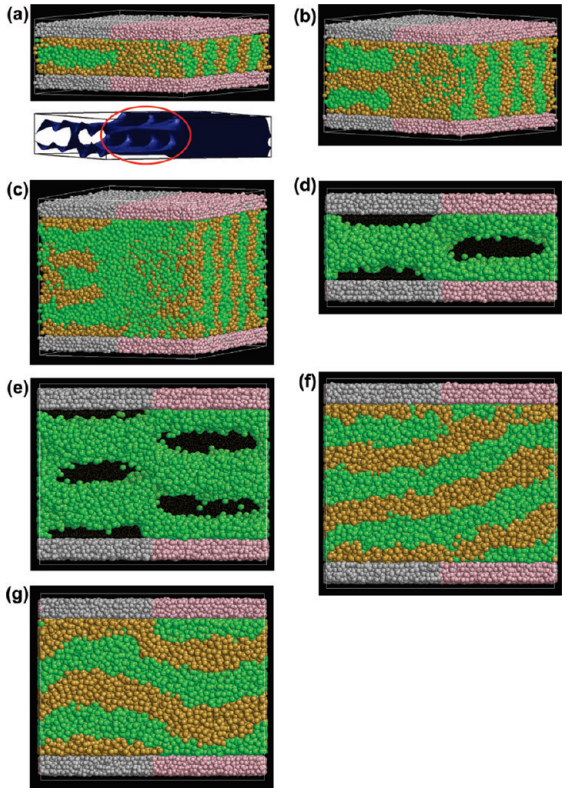

Figure 11. Examples of simulation configurations corresponding to Figure 10. (a) $L_{\parallel,1} + L_\perp$, (b) $L_{\parallel,2} + L_\perp$, (c) $L_{\parallel,3} + L_\perp$, (d) $L_{\parallel,1} + L_{\parallel,1}^{-1}$, (e) $L_{\parallel,2} + L_{\parallel,2}^{-1}$, (f) tilt-like lamellar phase, and (g) chevron-like lamellar phase. Shown in the inset of panel a are isosurfaces for the A beads together with Schrek's surface twist boundary indicted by a red oval. Green and gold spheres represent A and B beads, respectively, and gray and pink spheres represent w_1 and w_2 wall beads, respectively. B beads are not shown in panels d and e for visual clarity.

surface is generated by smoothly joining two sets of planes that are aligned normal with respect to each other.[27,28] (Schrek's surface twist boundary for the $L_{\parallel,1} + L_\perp$ phase is seen in the inset of Figure 11a.) The interface morphology of Schrek's surface minimizes the energy penalty at the boundary interface and thereby minimizes the overall energy of the A_5B_5 copolymers in the $L_{\parallel,\nu} + L_\perp$ phases.[12] The $L_{\parallel,\nu} + L_\perp$ phases prefer Schrek's surface twist boundary over a T-junction tilt boundary,[29] again because of the lower energy penalty at the boundary interface. For $W = (19)20$ when $\Delta a_{Bw_2}/\Delta a_{AB} = 0$, the influence of the w_2 walls is now so weak with respect to the other interactions that the system prefers to self-assemble into a parallel alignment, closely resembling its phase behavior in the planar slits without nanopatterns.

Overall, for the cases of $\Delta a_{Bw_2}/\Delta a_{AB} = 0.5$ and 1, once again, superposition behavior is followed where nanostructures with alternating parallel and inverse parallel lamellae are found (denoted as $L_{\parallel,1} + L_{\parallel,1}^{-1}$ and $L_{\parallel,2} + L_{\parallel,2}^{-1}$, where configuration snapshots are shown in Figure 11d,e, respectively). As observed previously in the $\Delta a_{Bw_2}/\Delta a_{AB} = 0.0$ case, relaxation of the system into perpendicular alignment between $L_{\parallel,1} + L_{\parallel,1}^{-1}$ and $L_{\parallel,2} + L_{\parallel,2}^{-1}$ is a result of the slit width not being commensurate with the bulk lamellae spacing. As also observed previously, for wide slit

(27) Thomas, E. L.; Anderson, D. M.; Henkee, C. S.; Hoffman, D. *Nature* **1988**, *334*, 598.
(28) Gido, S. P.; Gunther, J.; Thomas, E. L.; Hoffman, D. *Macromolecules* **1993**, *26*, 4506.
(29) Gido, S. P.; Thomas, E. L. *Macromolecules* **1994**, *27*, 6137.

widths the superposition behavior fails. For W = 18, 19, and 20 when $\Delta a_{Bw_2}/\Delta a_{AB}$ = 0.5, the systems self-assemble into tilt-like lamellar phases as shown in Figure 11f. For W between 16 to 20 when $\Delta a_{Bw_2}/\Delta a_{AB}$ = 1, we observed chevron-like lamellar phases (Figure 11g) instead of the expected $L_{\parallel,3} + L_{\parallel,3}^{-1}$. The simulation results in these wider slits indicate a weakened influence of the nanopatterns on the self-assembly because the tilt-like and chevron-like lamellae are similar to the $L_{\parallel,\nu}$ phases formed in planar slits without nanopatterns.

Additional DPD simulations with box lengths of L_x = 25 and L_y = 20 confirmed the self-assembled nanostructures obtained by the simulations with L_x = L_y = 25 except in the cases of [W, $\Delta a_{Bw_2}/\Delta a_{AB}$] = {[16,0], [19,0], [9,0.5]}, where the simulations relaxed to $L_{\parallel,2} + L_{\perp}$, $L_{\parallel,3} + L_{\perp}$, and $L_{\perp}$, respectively. Nanostructures determined from both simulation sizes are indicated in Figure 10, where the original size simulation result is shown first, separated by comma. All of these cases occur at microphase separation boundaries between two different types of nanostructures, which explains the ambiguity due to highly pronounced finite-size and commensurate effects.

The schematic phase diagram and some select nanostructures for narrow (L_{NP} = 6.25), vertically aligned nanopatterns together with a detailed discussion are left for the Supporting Information. Furthermore, examples of conformational behavior in terms of the nematic order parameter for the A_5B_5 copolymers confined in the vertically aligned nanopattern slits are also provided in the Supporting Information.

3.2.2. Planar Slits with Wide, Vertically-Staggered Nanopatterns. The schematic phase diagram and some select nanostructures for wide (L_{NP} = 12.5), vertically staggered nanopatterns are presented in Figures 12 and 13, respectively. Analogous to planar slits with vertically aligned, wide nanopatterns, generally the system self-assembles into nanostructures given by the superposition behavior of lamellar alignment in planar slits without nanopatterns (i.e., in the planar slits with w_1 and w_2 walls), with some exceptions for $\Delta a_{Bw_2}/\Delta a_{AB}$ = 0.5. We observed the formation of nanostructures given by the superposition of L and inverted L (denoted as L + iL, where a configuration snapshot is given in Figure 13a) and the superposition of $L-L_{\parallel,\nu}$ and inverted $L-L_{\parallel,\nu}$ with ν = 1 and 2 (denoted as $L-L_{\parallel,\nu}$ + $iL-L_{\parallel,\nu}$, where configuration snapshots at two different slit widths are given in Figure 13b,c). (Inverted adsorbed layer or inverted adsorbed layer−parallel lamellar phases differ from adsorbed layer or adsorbed layer−parallel lamellar phases simply by the adsorbed layer positioning with respect to the confining w_1 and w_2 walls. Thus, in our simulations, the adsorbed layer and adsorbed layer−parallel lamellar phases are confined by the upper w_1 wall and lower w_2 wall, and the positions of the w_1 and w_2 walls are inverted for the so-called inverted phases.) A unique nanostructure was observed for [W, $\Delta a_{Bw_2}/\Delta a_{AB}$] = [8, 0.5], where the system self-assembles into U-shape lamellae shown in Figure 13d. (This U-shape lamellar phase was also confirmed by a DPD simulation with box lengths of L_x = 25 and L_y = 20.) The U-shaped lamellar phase is evidently a transition structure between $L_{\perp}$ and $L-L_{\parallel,\nu}$ + $iL-L_{\parallel,\nu}$ that might exist in a narrow region of slit widths and system interaction parameters, satisfying a rather subtle balance between system interactions and block-wall adsorption energy. The weakened influence of the nanopatterns on the self-assembly is seen mainly for W > 16 and $\Delta a_{Bw_2}/\Delta a_{AB}$ = 0.5, where the systems exhibit chevron-like lamellar phases (Figure 13e). In contrast to the $\Delta a_{Bw_2}/\Delta a_{AB}$ = 0.5 case, systems with wide slit widths and $\Delta a_{Bw_2}/\Delta a_{AB}$ = 1 self-assemble into $L-L_{\parallel,2}$ + $iL-L_{\parallel,2}$, which nearly follows the superposition behavior of the parallel alignment. Additional

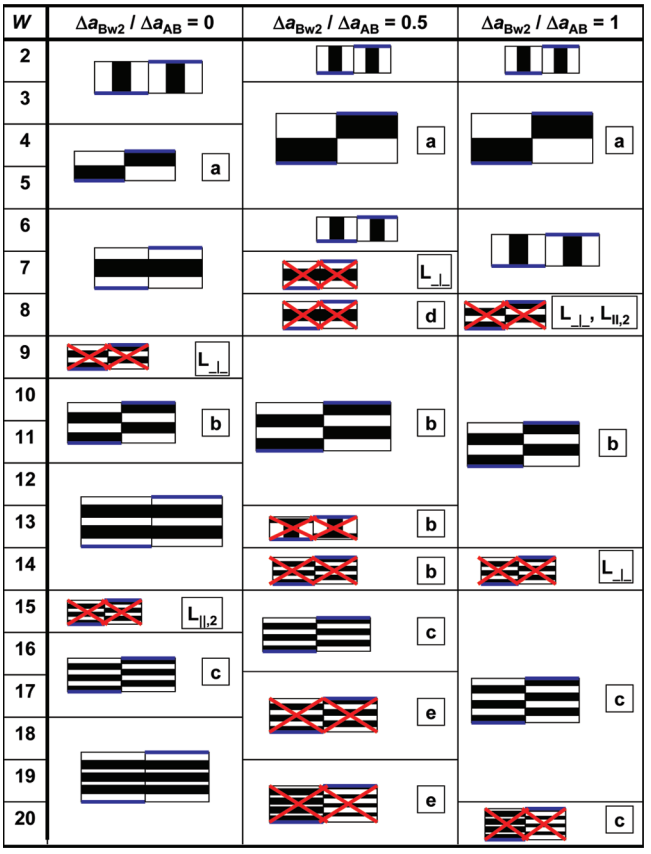

Figure 12. Self-assembly of the A_5B_5 systems confined in nanopatterned planar slits, where strips on opposing surfaces are vertically staggered with size L_{NP} = 12.5. W is the slit width, and $\Delta a_{Bw_2}/\Delta a_{AB}$ is a measure of phobicity of the B blocks toward the w_2 walls. Schematics indicate lamellar alignment in the planar slits without nanopatterns (i.e., in the planar slits with w_1 and w_2 walls). w_1 and w_2 walls are represented by black and blue lines, respectively. Crosses indicate cases where nanostructures did not result from the superposition of the lamellar alignment in the underlying planar slits without nanopatterns. Letters a−e refer to simulation configurations for some select nanostructures formed in the nanopatterned planar slits, which are shown in Figure 13. Other legend definitions are $L_{\perp}$, a perpendicular lamellar phase, and $L_{\parallel,2}$, a parallel lamellar phase with two A lamellae. For the case in which different nanostructures were observed for differently sized simulation cells, both nanostructures are shown, separated by a comma.

DPD simulations with box lengths of L_x = 25 and L_y = 20 lead to a different nanostructure only for the case of [W, $\Delta a_{Bw_2}/\Delta a_{AB}$] = [8, 1] (i.e., at the microphase-separation boundary between $L_{\perp}$ and $L-L_{\parallel,1}$ + $iL-L_{\parallel,1}$), where the system formed $L_{\parallel,2}$ rather than $L_{\perp}$. (Both nanostructures are indicated in Figure 12, separated by a comma).

The schematic phase diagram and some select nanostructures for narrow (L_{NP} = 6.25), vertically staggered nanopatterns together with a detailed discussion are left for the Supporting Information. Furthermore, examples of conformational behavior in terms of the nematic order parameter for the A_5B_5 copolymers confined in the vertically staggered nanopattern slits are also provided in the Supporting Information.

3.2.3. Planar Slits with Vertically Partially Staggered Nanopatterns. For vertically partially staggered nanopatterns, the self-assembly behavior does not follow the superposition description for either the narrow or the wide nanopatterns except in the cases of very narrow slit widths, where the systems form, in addition to the usual perpendicular lamellar phase, a novel

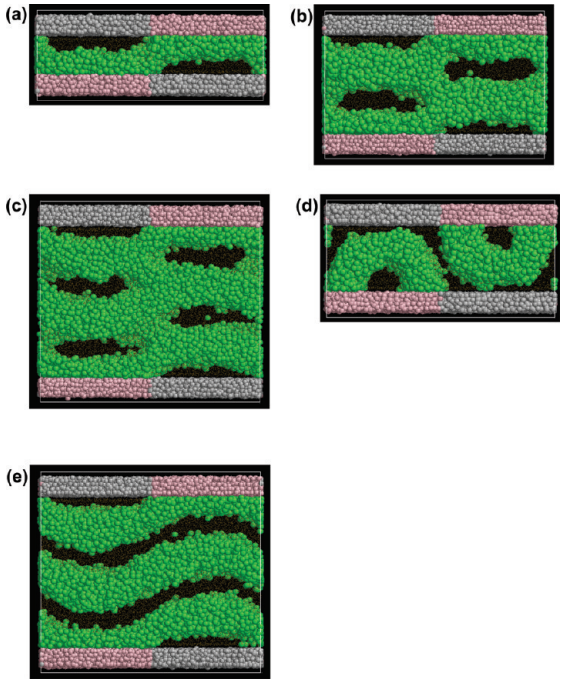

Figure 13. Examples of simulation configurations corresponding to Figure 12. (a) L + iL, (b) L−$L_{\|,1}$ + iL−$L_{\|,1}$, (c) L−$L_{\|,2}$ + iL−$L_{\|,2}$, (d) a U-shape lamellar phase, and (e) a chevron-like lamellar phase. Green spheres represent A beads, and gray and pink spheres represent w_1- and w_2-wall beads, respectively. B beads are not shown for visual clarity.

nanostructure given by a superposition of the adsorbed layer, the inverted adsorbed layer, and the perpendicular lamellar phases. For wide slits, the systems typically form tilt-like lamellar phases. The schematic phase diagram and some select nanostructures for vertically partially staggered nanopatterns together with a more detailed discussion are left for the Supporting Information.

3.3. Connection to Real Systems. Thus far in this work, all results are presented in reduced units with no connection to a real system. However, our DPD model of a symmetric diblock copolymer can be mapped onto actual symmetric diblock copolymers by establishing the physical values of the cutoff radius, r_c, the mass of a DPD bead, m_{DPD}, and the energy term k_BT by using, for example, a top-down coarse-grained approach.[30] Closely following the work in ref 30, we consider low-molecular-weight symmetric diblock copolymer poly(styrene-*b*-2-vinylpyridine) (PS-PVP) with an average molecular weight of 10 400 g mol^{-1} that consists of approximately 50 PS and 50 PVP monomers. Because our DPD diblock copolymer model corresponds to a flexible Gaussian chain composed of Kuhn segments,[31] the number of monomers defined by a Kuhn segment, C_∞, can be estimated using Bicerano's structural-relation method.[32] Following this procedure, we determine $C_\infty \simeq 9.9$ for both the PS and PVP blocks. Hence, a PS-PVP chain of 50 PS and 50 PVP monomers can be mapped onto a DPD chain of 5 A and 5 B beads, A_5B_5. Defining m_{mon} and V_{mon} as the average mass and average volume of the PS-PVP monomers, respectively, the mass and volume of a DPD bead can be determined from $m_{DPD} \approx C_\infty m_{mon} \simeq 1030$ g mol^{-1} and $V_{DPD} \approx C_\infty V_{mon} \simeq 1570$ Å^3, respectively. The value of r_c can be defined as the side of a cube containing an average number of ρ beads:

$$r_c = (\rho V_{DPD})^{1/3} \tag{18}$$

Equation 18 gives for the PS-PVP system $r_c \simeq 16.8$ Å. Using the established value of r_c, we can convert the geometry of the planar slits and simulation quantities such as R_e^2, R_g^2, W_{LAM}, and W_L into real units. For example, the slit widths in reduced units between 2 and 20 correspond to real values between 33.6 and 336 Å. Similarly, the size of the nanopatterned strips in reduced units, 6.25 and 12.5, correspond to real values 105 and 210 Å, respectively, which can be compared with the real value of the perpendicular-phase lamellae width of 54 Å (about 3.2 in reduced units).

The value of k_BT can be obtained by expressing χ_{AB}^{eff} in terms of the solubility parameters of the A(PS) and B(PVP) beads, δ_A and δ_B:[33]

$$\chi_{AB}^{eff} = \frac{V_{DPD}}{k_BT}(\delta_A - \delta_B)^2 \tag{19}$$

For the PS-PVP system, Bicerano's structural-relation method gives $\delta_A = 19.80$ (J cm^3)$^{1/2}$ and $\delta_B = 22.12$ (J cm^3)$^{1/2}$. Therefore, when $\chi_{AB}^{eff} \simeq 2$ is used in eq 19 we obtain $T = 300$ K and $k_BT \simeq 4 \times 10^{-21}$ J. To complete the mapping of our DPD confined diblock copolymer system onto a real system, one needs to relate our measures of phobicity between the diblock copolymer beads and the walls, $\Delta a_{Aw_1}/\Delta a_{AB}$ and $\Delta a_{Bw_2}/\Delta a_{AB}$, with the real interactions. In contrast to pure diblock copolymer systems, where mapping results from the correspondence between DPD and Flory−Huggins-type polymer models and solubility parameters, it is not a straightforward task to map the diblock−wall interactions. A possible route is by matching the DPD values of the surface tension for the block polymer−wall interfaces with the corresponding experimental values.[34] However, we leave such work to another study.

4. Conclusions

We performed a systematic study of model symmetric diblock copolymers A_5B_5 confined in planar slits with and without nanopatterns using DPD simulations. The DPD A_5B_5 copolymer can be considered to be a generic model for low-molecular-weight symmetric diblock copolymers such as the PS-PVP copolymer with an average molecular weight of 10 400 g mol^{-1} at 300 K. The nanopatterns were modeled by alternating portions of the slit surface that interacted differently with the diblock copolymer beads. We considered various nanopatterned slits where patterns on opposing surfaces were vertically (a) aligned, (b) staggered, and (c) partially staggered for two differently sized nanopatterns: 105 and 210 Å (or 6.25 and 12.5 in reduced units). We varied the slit width from 33.6 to 336 Å (or 2 to 20 in reduced units) and the diblock copolymer bead−wall interactions from preferential affinity to strong phobicity. We determined the confined phase behavior by analyzing equilibrium configurations in terms of bead-density profiles and isosurfaces, along with the coinciding characterization of the conformational behavior of the confined copolymers. We reiterate that the goal of this work was not to determine the precise location of the microphase separation boundaries but rather to investigate systematically and qualify the competing effects of physical adsorption and confinement on

(30) Malý, M.; Posocco, P.; Pricl, S.; Fermeglia, M. *Ind. Eng. Chem. Res.* **2008**, *47*, 5023–5038.
(31) Rubinstein, M.; Colby, R. H. *Polymer Physics*; Oxford University Press: London, 2006.
(32) Bicerano, J. *Prediction of Polymer Properties*; Marcel Dekker: New York, 2002.
(33) Prausnitz, J. M.; Lichtenthaler, R. N.; de Azevedo, E. G. *Molecular Thermodynamics of Fluid-Phase Equilibria*, 3rd ed., Prentice-Hall: New York, 1999.
(34) Maiti, A.; McGrother, S. *J. Chem. Phys.* **2004**, *120*, 1594–1601.

copolymer self-assembly, which to our knowledge is the first such study.

For the planar slits without nanopatterns, the systems self-assembled into perpendicular and parallel lamellar phases with different numbers of lamellae depending on the slit widths and the diblock copolymer bead−wall interactions. When the planar slits were composed of different types of opposing walls, the systems formed, in addition to the expected perpendicular and parallel lamellar phases, adsorbed layer and adsorbed layer−parallel lamellar phases, and a mixed lamellar phase. The observed phase behavior in the planar slits without nanopatterns closely correlated with the computed conformational characteristics of the diblock copolymers and with the widths of lamellae and adsorbed layers. For example, in the case where the B beads had a preferential affinity toward the slit walls the transformation between the parallel lamellar phases with different numbers of lamellae was accompanied by an elongation of the copolymers in the perpendicular direction, along with an increase in orientational order and an increase in the widths of lamellae and B-bead adsorbed layers.

The self-assembled behavior observed in the planar slits without nanopatterns enabled us to rationalize the self-assembly of the A_5B_5 copolymers in the nanopatterned planar slits because the nanopatterned planar slits can be virtually divided into portions that correspond to planar slits without nanopatterns. We investigated the applicability of superimposing the observed nanostructures in the planar slits without nanopatterns to predict the nanostructures formed when nanopatterns were present. For the planar slits with vertically aligned nanopatterns, the resulting nanostructures followed the superposition description quite well for wide nanopatterns and rather poorly for narrow nanopatterns. We observed two types of novel nanostructures given by (i) the superposition of parallel and perpendicular lamellar alignment with Schrek's surface twist boundary between the parallel and perpendicular domains and (ii) the superposition of parallel and inverse parallel lamellar phases. Similar to vertically aligned nanopatterns, the self-assembled nanostructures in the planar slits with vertically staggered nanopatterns obeyed the superposition description reasonably well for wide nanopatterns and poorly for narrow nanopatterns. Here, the systems exhibited two types of novel nanostructures given by (i) the superposition of adsorbed layer and inverted adsorbed layer phases and (ii) the superposition of adsorbed layer-parallel and inverted adsorbed layer-parallel lamellar phases. The system also formed a U-shaped lamellar phase in a narrow region of slit widths and system interaction parameters. For the planar slits with vertically partially staggered nanopatterns, the self-assembled nanostructures did not follow the superposition description for either narrow or wide nanopatterns except for very narrow slit widths. For these narrow slit widths, the systems formed, besides the usual perpendicular lamellar phase, a novel nanostructure given by the superposition of the adsorbed layer, inverted adsorbed layer, and perpendicular lamellar phases.

Acknowledgment. This research was supported by the Grant Agency of the Czech Republic (grant no. 203/08/0094), by the National Research Programme "Information Society" (project no. 1ET400720507), by the Grant Programme of the Academy of Sciences of the Czech Republic "Nanotechnology for Society" (project no. KAN400720701), and by the European Community under the sixth Framework Programme (project MULTIPRO no. 033304) and under the seventh Framework Programme (project COST TD0802).

Supporting Information Available: Phase diagram, some select nanostructures, and a detailed discussion of the diblock copolymer self-assembly behavior in the planar slits with narrow, vertically aligned, and narrow, vertically staggered nanopatterns as well as in the planar slits with vertically partially staggered nanopatterns. Examples of conformational behavior for the A_5B_5 copolymers confined in planar slits with vertically aligned and vertically staggered nanopatterns. This material is available free of charge via the Internet at http://pubs.acs.org.